Spatial Distribution of Lead iodide and Local Passivation on Organo-Lead Halide Perovskite

Sheng Chen,[a] Xiaoming Wen,[a,d] Jae S. Yun,[a] Shujuan Huang,[a] Martin Green[a], Nam Joong Jeon,[b] Woon Seok Yang,[c] Jun Hong Noh,[b] Jangwon Seo,[b] Sang Il Seok,[b,c*] Anita Ho-Baillie[a*]*

[a] Australia centre for Advanced Photovoltaics (ACAP). School of Photovoltaic and Renewable Energy Engineering, University of New South Wales, Sydney, New South Wales, 2052, Australia
[b] Division of Advanced Materials. Korea Research Institute of Chemical Technology. 141 Gajeong-Ro, Yuseong-Gu, Deajeon 305-600, South Korea
[c] School of Energy and Chemical Engineering. Ulsan National Institute of Science and Technology (UNIST)
[d] Centre for Micro-Photonics, Swinburne University of Technology, Melbourne 3122, Australia

KEYWORDS: perovskite, nanoscale, PbI_2, passivation, lifetime

ABSTRACT: We identify nanoscale spatially distribution of PbI_2 on the $(FAPbI_3)_{0.85}(MAPbBr_3)_{0.15}$ perovskite thin film and investigate the local passivation effect using confocal based optical microscopy of steady state and time-resolved photoluminescence (PL). Different from typical scanning electron microscope (SEM) morphology study, confocal based PL spectroscopy and microscopy allow to map the morphologies of both perovskite and PbI_2 grains simultaneously, by selectively detecting their characteristic fluorescent bands using band-pass filters. In this work, we compare the perovskite samples without and with excess PbI_2 incorporation and unambiguously reveal PbI_2 distribution for the excess PbI_2 sample. In addition, using nanoscale time-resolved PL technique we show that the rich- PbI_2 regions exhibit longer lifetime due to suppressed defect trapping, compared to the less- PbI_2 regions. The measurement on PbI_2 excess sample indicates that the passivation effect of PbI_2 in perovskite film is effective, especially in localised regions. Hence, this finding is important for further improvement of the solar cells by considering the strategy of excess PbI_2 incorporation.

INTRODUCTION

As an absorber layer in solar cells, organo-lead halide perovskites have achieved rapid development and remarkable power conversion efficiency (PCE) over 20%.[1-5] In addition, the advantages of simple fabrication, tunable band gap and superior photonic properties make them competitive compared to conventional silicon solar cells.[6-12] As the work on improving efficiency attracts the most of attentions, a well-known optimisation method is to reduce the defect states in perovskite film. Recently, the effect of lead iodide attracts many attentions due to its conflicting properties. In 2014, Chen and co-workers proposed that PbI_2 have the passivation effect on the perovskite film after further annealing at 150 °C, which is beneficial to the device performance.[13] Moreover, Kim *et al*. have shown that an enhanced PCE of $(FAPbI_3)_{0.85}(MAPbBr_3)_{0.15}$ with 5.7 mol% PbI_2 incorporated, compared to the device without excess PbI_2 incorporated.[14] Jacobsson *et al.* proposed that PbI_2-sufficient sample had higher efficiency but PbI_2-deficient sample appeared more homogeneous and better crystal quality.[15] However, PbI_2 is also a product of the degradation of $MAPbI_3$ and $FAPbI_3$, which forms volatile molecular defects.[16-19] Yuan *et al.* demonstrated the decomposition of perovskite can generate extra PbI_2 after applying an electrical field.[20] This means that PbI_2 is probably a sign of instability of perovskite material.[21] Therefore the controversial nature of the incorporation of excess PbI_2 necessitates further study to understand how it influences the perovskite film.

Current characterization of existence of PbI_2 is commonly done by X-ray diffraction (XRD), scanning electron microscope (SEM) and the Kelvin probe force microscopy (KPFM).[13-14, 21] XRD is an effective technique for detection of the PbI_2 existence. SEM and KPFM images can identify the PbI_2-like regions through showing the contrast and contact potential difference. However, it still requires a characterization technique combined with the elemental mapping ability and carrier dynamics analytical system for deeper understanding the PbI_2 influence on the perovskite film. Recently, Jacobsson *et al.* used photoluminescence (PL) technique to obtain the morphology of perovskites in different PbI_2 content based on the perovskite emission.[15] In this report, we acquire the morphologies of both lead iodide and perovskite simultaneously by selectively detecting the emission bands of lead iodide and perovskite using confocal PL microscopy. We identify unambiguously the spatial distribution of lead iodide on PbI_2 rich $(FAPbI_3)_{0.85}(MAPbBr_3)_{0.15}$ perovskite film and further confirm their effect of passivation combined with time-correlated

single photon counting (TCSPC) technique. The advantage of the PL microscopy is that it allows the identification of the measured materials by the "spectral signatures" of the perovskite and PbI_2 simultaneously. Using this method, we observe that PbI_2 embed in between of the $(FAPbI_3)_{0.85}(MAPbBr_3)_{0.15}$ grains and study the interaction between PbI_2 and perovskite grains in nanoscale. Results from the local time-resolved PL on the perovskite film suggest that PbI_2 can locally passivate the defect states of the perovskite film. Moreover, we confirm the $(FAPbI_3)_{0.85}(MAPbBr_3)_{0.15}$ perovskite with excess PbI_2 exhibits a longer carrier lifetime than the perovskite film without excess PbI_2. It indicates that PbI_2 can effectively passivate the defect states of the perovskite film, consistent to the previous publications.[13-15, 21] These findings are important for further improvement of the solar cells by considering the strategy of excess PbI_2 incorporation.

Experimental Section

Material synthesis and sample prepare

Firstly, $NH_2CH=NH_2I$ was synthesized by reacting 30 ml hydroiodic acid (57% in water, Aldrich), 27.86 ml CH_3NH_2 (40% in methanol, Junsei Chemical), and 15 g formamidine acetate (Aldrich) in a 250 ml round-bottomed flask at 0 °C for 2 h with stirring. The precipitates were recovered by evaporating the solutions at 50 °C for 1 h. The products were dissolved in ethanol, recrystallized using diethyl ether, and finally dried at 60 °C in a vacuum oven for 24 h. Similarly, CH_3NH_3Br was prepared using hydrobromic acid (48 wt% in water, Aldrich). Then, the 1.05 M solutions dissolving $NH_2CH=NH_2I$ and CH_3NH_3Br with PbI_2 and $PbBr_2$ in *N*-*N*-dimethylformamide (=DMF) and dimethylsulfoxide (=DMSO) = (6:1 v/v). The additional PbI_2 was added in the solution and the mole ratio of PbI_2 to $(FAPbI_3)_{0.85}(MAPbBr_3)_{0.15}$ were 0 and 5.7 mol%. The final products were then coated onto the mesoporous-TiO_2 /blocking-TiO_2 /FTO substrate heated to 50 °C by two consecutive spin-coating steps, at 1000 and 5000 rpm for 5 and 10 s, respectively.

Spectroscopic measurements

Steady state PL was measured by a spectrometer, detected with a Si-CCD detector and with excitation of 405 nm. The photoluminescence images were obtained by a Leica TCS SP5 microscopy. The continuous wave argon-ion laser with 458 nm was used to excite the sample. For the PbI_2 image, the detection of band was selected in a range of 515/50 nm. For the $(FAPbI_3)_{0.85}(MAPbBr_3)_{0.15}$ image, the detection of band was modified to 770/50 nm. The local PL decay traces were measured in Microtime-200 (PicoQuant) with excitation of 470 nm laser and detection through 525/50 nm and 750/40 nm bandpass filter. 100 x Oil objective with NA1.4 was used in the experiment. All the PL experiments were undertaken at room temperature and the humidity was less than 50 %. XRD patterns were measured using a PANalytical Xpert Materials Research diffractometer system with a Cu Kα radiation source (λ = 0.1541 nm) at 45 kV and 40 mA. KPFM measurements were carried out using an AFM (AIST-NT SmartSPM^{TM}) in air, using a gold coated Si tip with a 6 nm radius of curvature (HYDRA6R-100NG-10, APPNANO) with an AC voltage of -1 to +1 V. Nitrogen gun was used to remove particles from sample surfaces prior to the measurements. Samples were measured immediately after they were removed from nitrogen storage. Consistent results have been achieved from repetitive measurements over 10 hours.

RESULTS AND DISCUSSION

To investigate the spatial distribution and the influence of PbI_2, a $(FAPbI_3)_{0.85}(MAPbBr_3)_{0.15}$ perovskite film with 0 mol% and 5.7 mol% PbI_2 incorporated on the mesoporous-TiO_2/ blocking- TiO_2/ FTO glass substrates are fabricated.[14, 22] The fabrication details are presented in the experimental section and such fabricated perovskite based solar cells have been previously reported to achieve conversion efficiency as high as 20.1 %.[14] The detailed current-voltage characterizations are also reported in the publication. In this work, the PL spectra of the perovskite film excited at 405 nm and measured by a spectrometer with a Si-CCD detector, as shown in Figure 1 (a). Previous works have shown the formation of crystalline PbI_2 in the perovskite film, where X-ray diffraction (XRD) pattern is used as main characterization tool to identify the existence of PbI_2.[13-14, 16, 21, 23-24] In our study, evident PbI_2 peak is observed at 12.67 ° from the XRD pattern for the 5.7 mol% sample; see Figure 1 (b).[14] Figure 1 (c) and (d) are the SEM images of the 5.7 mol% and 0 mol% PbI_2 incorporated perovskite film surface. As shown in the image, the 5.7 mol% sample contains small grains around large perovskite grains (700-1000 nm). Such small grains are generally speculated as PbI_2 as a result of inserting excess PbI_2 into the perovskite solution.[13, 25-26] In order to gain further insight into these grains, KPFM and confocal PL microscopy measurement are conducted.

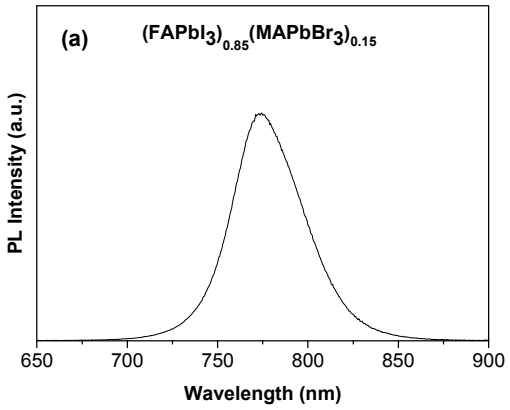

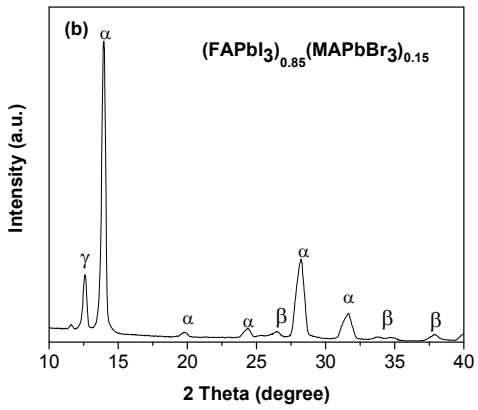

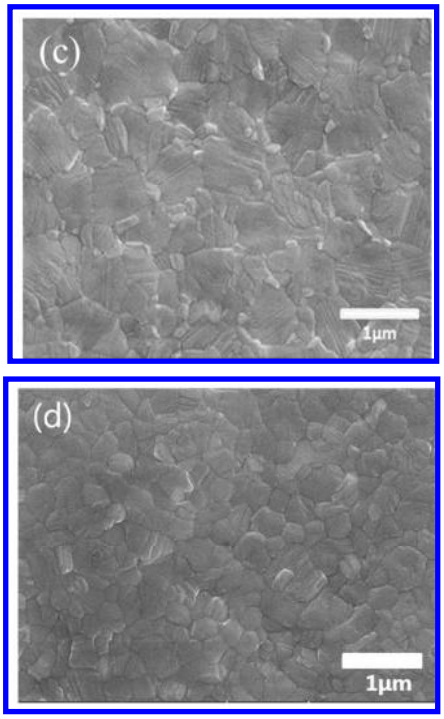

Figure 1. (a) The PL spectrums of solvent-engineering-processed $(FAPbI_3)_{0.85}(MAPbBr_3)_{0.15}$ film, on mesoporous-TiO_2/ blocking- TiO_2/ FTO glass substrates. (b) XRD spectra of the $(FAPbI_3)_{0.85}(MAPbBr_3)_{0.15}$ film with 5.7 mol% PbI_2 incorporation. XRD peaks are labelled for perovskite (α), FTO (β) and PbI_2 (γ). (c) SEM of the perovskite film with incorporation of PbI_2. (d) SEM of $(FAPbI_3)_{0.85}(MAPbBr_3)_{0.15}$ with 0 mol% PbI_2.

Figure 2 (a) shows the topography and contact potential difference spatial maps of a 16 μm^2 area of the 5.7 mol% PbI_2 sample measured in the dark. Interestingly, there are some grains randomly distributed over the full area which have relatively low contact potential difference (CPD) and marked by the circles in the CPD map of Figure 2 (a). SEM image of the film shows a similar feature where there are some grains which have relatively lighter contrast compared to other grains. A CPD map directly reflects distribution of the work function differences so we suspect that these grains have different compositions. Figure 2 (b) shows topography and CPD profile of the same grains in Figure 2 (a). It is apparent that the CPD and topography profiles do not have same profile which ensures that our CPD measurement is not a direction correlation with the topographical feature. Rather, it clearly indicates that the bulk of this grain has relatively lower CPD (20-25 mV) compare to other grains. Also, these grains commonly have even lower CPD compare to the CPD at the grain boundaries which is found to be 5-15 mV lower CPD that the grain interior reported earlier.[14] Therefore, we speculate that can be PbI_2 as these grains have their unique electrical properties and the morphology of this crystal resembles the hexagonal PbI_2 crystal reported elsewhere.[27]

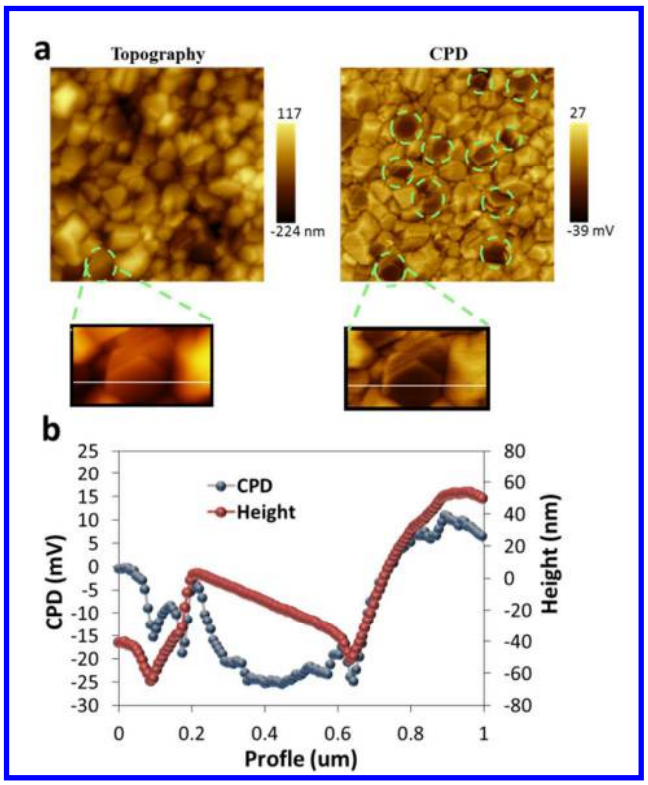

Figure 2. Topography and CPD analysis for suspected PbI_2 grains. (a) Topography map and corresponding CPD map of a 16 μm^2 area. (b) Topography and CPD line profile of a region represented by a white line from inset of (a).

Further identification of these suspected PbI_2 grains can be achieved by using PL microscopy (Leica TCS SP5). We prepare a pure PbI_2 deposited on a glass and measure the PL spectra, as shown in Figure 3 (a). Then we measure the PL spectra of the 5.7 mol% PbI_2 perovskite sample at the short wavelength regime (480 ~ 600 nm) with excitation at 458 nm, as shown in Figure 3 (b). An evident PL peak is identified close to 510 nm which is consistent to the pure PbI_2 sample.[13, 28] Meanwhile, we measure the lifetime of the PL decay at 510 nm, as shown in the inset of Figure 3 (b) and the lifetime of 0.7 ns is obtained. This is consistent with the previous report.[28] Figures 3 (c) and (d) shows the PL images detected at 510 nm and at

770 nm, corresponding to the emissions of PbI_2 and perovskite, respectively. Figure 3 (e) is an overlay image of the 3 (c) and 3 (d). In Figure 3 (c), the red area indicates the high emission at 510 nm and thus signifies local accumulation of PbI_2 (rich- PbI_2 region). Similarly in Figure 3 (d), the light blue area indicates the higher emission of $(FAPbI_3)_{0.85}(MAPbBr_3)_{0.15}$ at 770nm (less- PbI_2 region). On the other hand, in PL image (Figure 3 (d)) the dark regions represent the low PL intensity. Essentially, this can be ascribed to less perovskite in the areas or low PL quantum efficiency; the latter will be excluded by the time-resolved PL measurement, as discussed later. When we overlay the PL image of PbI_2 and the PL image of $(FAPbI_3)_{0.85}(MAPbBr_3)_{0.15}$, the local rich- PbI_2 regions fit into the dark area of $(FAPbI_3)_{0.85}(MAPbBr_3)_{0.15}$ perfectly; see Figure 3 (e). It highly suggests that PbI_2 is locally accumulated in between of perovskite grains. Thus, those perovskite grain boundaries are influenced by the PbI_2 easily, consistent to the previous work.[14, 29] It should be noted that the PbI_2 has much lower PL emission than the perovskite, due to the lower concentration and lower PL efficiency of the PbI_2 in the film.

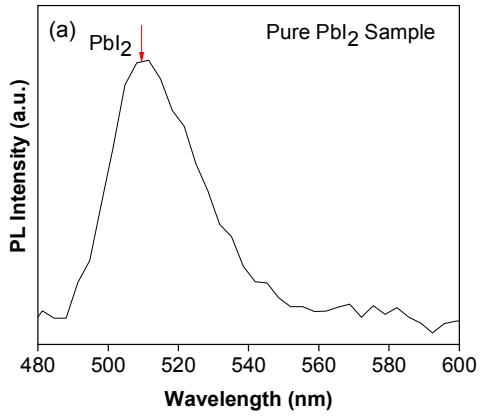

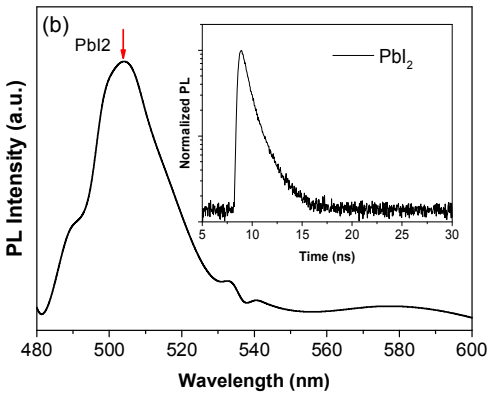

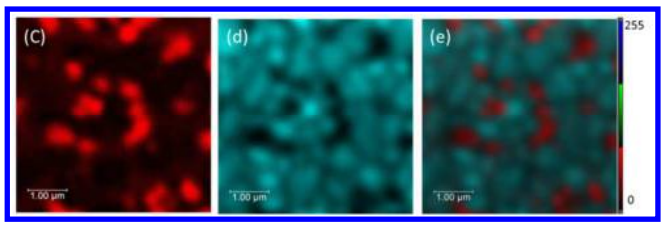

Figure 3. The PL spectra of the (a) pure PbI_2 sample (b) observed PbI_2 peak from the perovskite film; Inset is the PL decay trace of PbI_2. PL images of the identical area detection (c) at 510 nm; (d) at 770 nm; (e) an overlay image of (c) and (d).

To obtain further insight into the microscopic mechanism of the influence of PbI_2, we perform a fluorescence lifetime imaging microscopy (FLIM) to provide nanoscale spatially- and lifetime-resolved morphology. Figure 4 shows the FLIM images of the film detected (a) at 770 nm (highlighting $(FAPbI_3)_{0.85}(MAPbBr_3)_{0.15}$ regions) and (b) at 510 nm (highlighting PbI_2 regions) under 470 nm excitation, respectively. Figure 4 (c) and (d) show the corresponding PL intensity images. These images allow the location of less- PbI_2 (red square) and rich- PbI_2 regions (green square), for subsequent local time-resolved PL via confocal PL technique. Figure 4 (e) compares the PL decay traces of perovskite detection at 770 nm between the less- PbI_2 (the red square) and rich- PbI_2 regions (the green square). Typically, the carrier dynamics of perovskite can be expressed as:[30-31]

$$\frac{dn}{dt} = C_1 n + C_2 n^2 + C_3 n^3 \qquad (1)$$

where the terms represent as defect trapping (Shockley-Read-Hall recombination), free electron-hole recombination and Auger recombination, respectively. Note the sample is excited at low intensity of 50 mW/cm^2 with repetition rate of 5 MHz. At a low excitation, the fast and slow components are attributed to the defect trapping and e-h recombination but Auger recombination is negligible.[6, 30-31] For the PL decay traces in Figure 4 (e), a bi-exponential decay function (2) and the effective lifetime (3) are used to perform the quantitative analysis. [32]

$$y = A_1 \exp(-\frac{t}{\tau_1}) + A_2 \exp(-\frac{t}{\tau_2}) \qquad (2)$$

$$\tau_{eff} = \frac{A_1\tau_1 + A_2\tau_2}{A_1 + A_2} \qquad (3)$$

The fitting parameters and effective lifetimes are summarised in Table 1. Note that the detection band is at 770 nm, corresponding to perovskite emission. The PL decay trace of the less- PbI_2 point shows a very fast component which is associated with defect trapping,[33] compared to the point of rich- PbI_2. It has been confirmed that higher defect trapping will exhibit a faster component in PL decay trace in perovskites.[34-35] It is necessary to emphasize that the time resolution of the used TCSPC system is 0.15 ns determined by response function, much shorter than the lifetime of the fast component (~ 10 ns). Thus, the results signify that the defect trapping plays a significant role of the carrier lifetime when the localized perovskite grain contains none or less PbI_2. Table 1 clearly shows that the area with rich- PbI_2 exhibits evidently longer

lifetime (197 ns) than the area with less- PbI_2 (120 ns). Moreover, the PbI_2 rich area displays much lower weight ratio of defect trapping (~ 5 %), compared to the other point with the weight ratio of 25 %. This clearly indicates that with rich- PbI_2 the perovskite exhibit significantly decreased defect trapping and therefore increased lifetime. We have measured multiple points and all exhibit a consistent result with fluctuation of 20%. These results are highly suggestive of the variations in local density of defect states due to the existence of PbI_2.

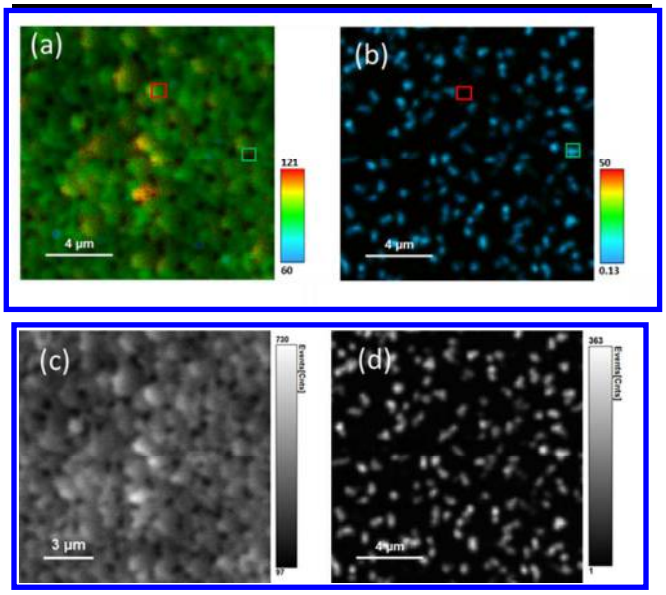

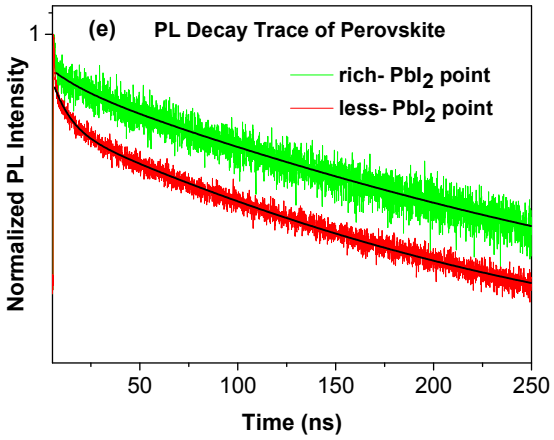

Figure 4. FLIM images of perovskite film detection (a) at 770 nm (highlighting $(FAPbI_3)_{0.85}(MAPbBr_3)_{0.15}$ regions) and (b) at 510nm (highlighting PbI_2 regions), with lifetime scale bar in nanosecond. PL intensity images of film (c) at 770nm, and (d) at 510nm. (e) PL decay curves of 770 nm emissions from rich- PbI_2 region (green square) and less- PbI_2 region (red square).

Table 1. The comparison of PL decay fitting parameters between rich- PbI_2 and less- PbI_2 regions on perovskite film at 770 nm.

$(FAPbI_3)_{0.85}(MAPbBr_3)_{0.15}$	Less- PbI_2	Rich- PbI_2
τ_1 (ns)	8.2	16.4
τ_2 (ns)	158.0	206.5
τ_{eff} (ns)	120.9	197.3
Weight of the fast component (%)	25	5

To explore the influence of PbI_2 on the carrier dynamics in perovskite film, we prepare a 0 mol% PbI_2 incorporated sample with identical procedure for comparison. As shown in the Figure 1 (d), there is no PbI_2 grain observed in the surface compared to the perovskite film with extra PbI_2 shown in Figure 1 (c) (white particle), consistent to previous publication.[14] Then, we measure the PL decay traces of two samples over a 25 μm^2 area under the same excitation intensity of 100 mW/cm^2; see Figure 5 (b). The effective lifetime of the 5.7 mol% sample (black) is around 400 ns, which is evidently longer than the 0 mol% sample (red) with the effective lifetime of 270 ns. This observation suggests that the incorporation of PbI_2 has passivation effect and results in carrier lifetime increase. Note the lifetime between the point and the area measurement can be different which is due to the different excitation intensity and the surface inconsistency.[6, 30-31]

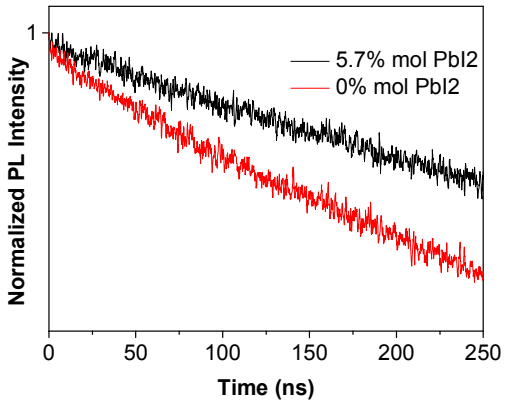

Figure 5. PL decay traces of 5.7 mol% (black) and 0 mol% (red) PbI_2 added perovskite film.

The PL microscopy combined with time-resolved PL technique is capable of mapping the spatially distribution and therefore analysing the local influence of PbI_2 on perovskite grains and impact on the local carrier dynamics. The PbI_2 effects in perovskite solar cells has been investigated based on SEM microscopy. Chen *et al.* proposed the PbI_2 has the passivation effect on the perovskite film.[13] Recently, Zhang *et al.* provided further evidences to support the effect by direct reaction of hydrohalide deficient PbI_2·xHI/Br precursors with MA followed by annealing.[25] They found the sample with PbI_2 exhibited longer lifetime and higher open-circuit voltage which is likely due to PbI_2 passivation. Our observations re-

veal clearly that rich- PbI_2 grains can locally passivate the perovskite film. At the rich- PbI_2 regions, the defect trapping is significantly suppressed, which can be attributed to the decreased trapping states and/or surface trapping states. We propose a possible carrier dynamics for the PbI_2-rich regions as shown in the Figure 6: the incident light excites the carriers from the valence band to the conduction band and then the hot carriers cool down to the lower level of the conduction band. Some of the carriers recombine with holes and generate radiative emission (PL) but the rest of them are trapped by the defects. It is generally accepted that the surface passivation can effectively decrease the defect or surface trapping states and thus suppress the defect trapping, such as in colloidal quantum dots.[36] In the figure, the defect suppression represents as an overlap of PbI_2 and unoccupied defect (white circle). Therefore, the effective lifetime in rich- PbI_2 regions is much longer than that in less- PbI_2 regions, see Table 1. Based on these results, we conclude that PbI_2 is beneficial to the suppression of defect trapping by passivation of the perovskite film. It has been shown that suitable extra PbI_2 can improve the conversion efficiency of perovskite based solar cells.[14] However, PbI_2 embed in between of perovskite grains and so the passivation effect is local distribution. Hence, optimization of the PbI_2 coverage seems to be a plausible way to improve the performance of solar cell and other effects of the excess PbI_2 has also been considered. Nevertheless, further investigation and deep physical understanding for the detailed mechanism of interface passivation is very necessary.

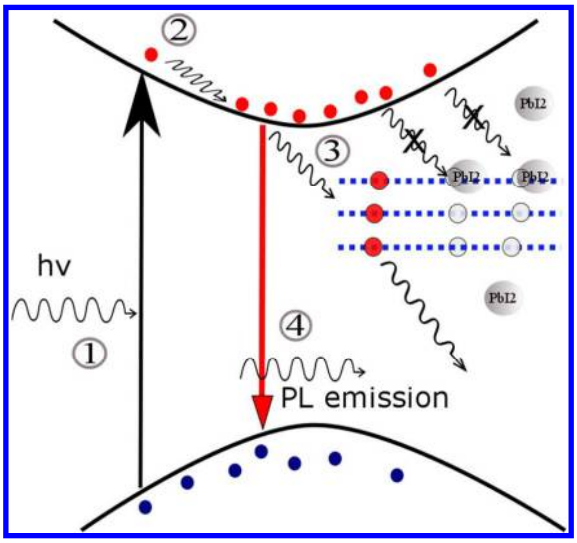

Figure 6. Schematic carrier dynamic processes and passivation of PbI_2 – lead iodide results in suppression of defect trapping, (1) photoexcitation and generation of hot carriers; (2) carrier cooling; (3) trapping of carriers (red circle); (4) carriers radiative recombination.

CONCLUSIONS

We have characterised the spatially distribution of PbI_2 on an 5.7 mol% PbI_2 incorporated perovskite film $(FAPbI_3)_{0.85}(MAPbBr_3)_{0.15}$ and investigated its effect on the carrier dynamics of the film using confocal based PL/TRPL spectroscopy and microscopy. We observe the spatially distribution of PbI_2 and $(FAPbI_3)_{0.85}(MAPbBr_3)_{0.15}$ perovskite simultaneously based on their PL signatures. We clearly show the formation of rich- PbI_2 grains are in between of $(FAPbI_3)_{0.85}(MAPbBr_3)_{0.15}$ grains. These rich- PbI_2 grains exhibit a different contact potential compared to the perovskite grain through KPFM analysis, indicating the grains have their unique electrical property. In addition to mapping PbI_2 distribution on perovskite film, we apply a local time-resolved PL measurement between the rich- PbI_2 and less- PbI_2 grains. Upon the analysis of the PL decay traces, we confirm that the perovskites in rich- PbI_2 grains exhibit longer lifetime due to the suppression of the defect trapping. It is necessary to emphasize that such passivation effect is locally distributed. Therefore, to increase the PbI_2 content selectively at the interfaces or grain boundaries rather than distributing throughout the film may be an optimized method of improving the solar cell performance. However, the stability of the perovskite device with excess PbI_2 incorporated is still a debatable topic which requires further investigation.

AUTHOR INFORMATION

Corresponding Author

* Xiaoming Wen; E-mail: x.wen@unsw.edu.au
Sang Il Seok; E-mail: seoki@unist.ac.kr
Anita Ho-Baillie; E-mail: a.ho-baillie@unsw.edu.au

Notes

The authors declare no competing financial interests.

ACKNOWLEDGMENT

The Australian Centre for Advanced Photovoltaics (ACAP) encompasses the Australian-based activities of the Australia-US Institute for Advanced Photovoltaics (AUSIAPV) and is supported by the Australian Government through the Australian Renewable Energy Agency (ARENA).

S.I. Seok and J.H. Noh acknowledge the financial support from by the National Research Foundation of Korea (NRF) grants funded by the Ministry of Science, ICT & Future Planning (MSIP) of Korea under contract number. NRF-2011-0031565 (Global Frontier R&D Program for Multiscale Energy System), and NRF-2015M1A2A2056542 (climate change program).

REFERENCES

1. Kojima, A.; Teshima, K.; Shirai, Y.; Miyasaka, T., Organometal Halide Perovskites as Visible-Light Sensitizers for Photovoltaic Cells. *J. Am. Chem. Soc.* **2009,** *131* (17), 6050-6051.
2. Kim, H.-S.; Lee, C.-R.; Im, J.-H.; Lee, K.-B.; Moehl, T.; Marchioro, A.; Moon, S.-J.; Humphry-Baker, R.; Yum, J.-H.; Moser, J. E.; Gratzel, M.; Park, N.-G., Lead Iodide Perovskite

Sensitized All-Solid-State Submicron Thin Film Mesoscopic Solar Cell with Efficiency Exceeding 9%. *Sci. Rep.* **2012,** *2*, 591.

3. Burschka, J.; Pellet, N.; Moon, S.-J.; Humphry-Baker, R.; Gao, P.; Nazeeruddin, M. K.; Gratzel, M., Sequential deposition as a route to high-performance perovskite-sensitized solar cells. *Nature* **2013,** *499* (7458), 316-319.

4. Lee, M. M.; Teuscher, J.; Miyasaka, T.; Murakami, T. N.; Snaith, H. J., Efficient Hybrid Solar Cells Based on Meso-Superstructured Organometal Halide Perovskites. *Science* **2012,** *338* (6107), 643-647.

5. Yang, W. S.; Noh, J. H.; Jeon, N. J.; Kim, Y. C.; Ryu, S.; Seo, J.; Seok, S. I., High-performance photovoltaic perovskite layers fabricated through intramolecular exchange. *Science* **2015,** *348* (6240), 1234-1237.

6. Stranks, S. D.; Burlakov, V. M.; Leijtens, T.; Ball, J. M.; Goriely, A.; Snaith, H. J., Recombination Kinetics in Organic-Inorganic Perovskites: Excitons, Free Charge, and Subgap States. *Phys. Rev. Appl.* **2014,** *2* (3), 034007.

7. Xing, G.; Mathews, N.; Sun, S.; Lim, S. S.; Lam, Y. M.; Grätzel, M.; Mhaisalkar, S.; Sum, T. C., Long-Range Balanced Electron- and Hole-Transport Lengths in Organic-Inorganic CH3NH3PbI3. *Science* **2013,** *342* (6156), 344-347.

8. Sheng, R.; Ho-Baillie, A.; Huang, S.; Chen, S.; Wen, X.; Hao, X.; Green, M. A., Methylammonium Lead Bromide Perovskite-Based Solar Cells by Vapor-Assisted Deposition. *J. Phys. Chem. C* **2015,** *119* (7), 3545-3549.

9. Hodes, G., Perovskite-Based Solar Cells. *Science* **2013,** *342* (6156), 317-318.

10. Mingzhen, L.; Johnston, M. B.; Snaith, H. J., Efficient planar heterojunction perovskite solar cells by vapour deposition. *Nature* **2013,** *501* (7467), 395-398.

11. Zuo, C.; Bolink, H. J.; Han, H.; Huang, J.; Cahen, D.; Ding, L., Advances in Perovskite Solar Cells. *Adv. Sci.* **2016,** *3* (7), DOI: 10.1002/advs.201500324.

12. De Wolf, S.; Holovsky, J.; Moon, S.-J.; Löper, P.; Niesen, B.; Ledinsky, M.; Haug, F.-J.; Yum, J.-H.; Ballif, C., Organometallic Halide Perovskites: Sharp Optical Absorption Edge and Its Relation to Photovoltaic Performance. *The J. Phys. Chem. Lett.* **2014,** *5* (6), 1035-1039.

13. Chen, Q.; Zhou, H.; Song, T.-B.; Luo, S.; Hong, Z.; Duan, H.-S.; Dou, L.; Liu, Y.; Yang, Y., Controllable Self-Induced Passivation of Hybrid Lead Iodide Perovskites toward High Performance Solar Cells. *Nano Lett.* **2014,** *14* (7), 4158-4163.

14. Kim, Y. C.; Jeon, N. J.; Noh, J. H.; Yang, W. S.; Seo, J.; Yun, J. S.; Ho-Baillie, A.; Huang, S.; Green, M. A.; Seidel, J.; Ahn, T. K.; Seok, S. I., Beneficial Effects of PbI2 Incorporated in Organo-Lead Halide Perovskite Solar Cells. *Adv. Energy Mater.* **2016,** *6* (4), DOI: 10.1002/aenm.201502104.

15. Jacobsson, T. J.; Correa-Baena, J.-P.; Halvani Anaraki, E.; Philippe, B.; Stranks, S. D.; Bouduban, M. E. F.; Tress, W.; Schenk, K.; Teuscher, J.; Moser, J.-E.; Rensmo, H.; Hagfeldt, A., Unreacted PbI2 as a Double-Edged Sword for Enhancing the Performance of Perovskite Solar Cells. *J. Am. Chem. Soc.* **2016**, DOI: 10.1021/jacs.6b06320.

16. Deretzis, I.; Alberti, A.; Pellegrino, G.; Smecca, E.; Giannazzo, F.; Sakai, N.; Miyasaka, T.; La Magna, A., Atomistic origins of CH3NH3PbI3 degradation to PbI2 in vacuum. *Appl. Phys. Lett.* **2015,** *106* (13), 131904.

17. Smecca, E.; Numata, Y.; Deretzis, I.; Pellegrino, G.; Boninelli, S.; Miyasaka, T.; La Magna, A.; Alberti, A., Stability of solution-processed MAPbI3 and FAPbI3 layers. *Phys. Chem. Chem. Phys.* **2016,** *18*, 13413-13422.

18. Frost, J. M.; Butler, K. T.; Brivio, F.; Hendon, C. H.; van Schilfgaarde, M.; Walsh, A., Atomistic Origins of High-Performance in Hybrid Halide Perovskite Solar Cells. *Nano Lett.* **2014,** *14* (5), 2584-2590.

19. Alberti, A.; Deretzis, I.; Pellegrino, G.; Bongiorno, C.; Smecca, E.; Mannino, G.; Giannazzo, F.; Condorelli, G. G.; Sakai, N.; Miyasaka, T.; Spinella, C.; La Magna, A., Similar Structural Dynamics for the Degradation of CH3NH3PbI3 in Air and in Vacuum. *ChemPhysChem* **2015,** *16* (14), 3064-3071.

20. Yuan, Y.; Wang, Q.; Shao, Y.; Lu, H.; Li, T.; Gruverman, A.; Huang, J., Electric-Field-Driven Reversible Conversion Between Methylammonium Lead Triiodide Perovskites and Lead Iodide at Elevated Temperatures. *Adv. Energy Mater.* **2016,** *6* (2), DOI: 10.1002/aenm.201501803.

21. Liu, F.; Dong, Q.; Wong, M. K.; Djurišić, A. B.; Ng, A.; Ren, Z.; Shen, Q.; Surya, C.; Chan, W. K.; Wang, J.; Ng, A. M. C.; Liao, C.; Li, H.; Shih, K.; Wei, C.; Su, H.; Dai, J., Is Excess PbI2 Beneficial for Perovskite Solar Cell Performance? *Adv. Energy Mater.* **2016,** *6* (7), DOI: 10.1002/aenm.201502206.

22. Jeon, N. J.; Noh, J. H.; Yang, W. S.; Kim, Y. C.; Ryu, S.; Seo, J.; Seok, S. I., Compositional engineering of perovskite materials for high-performance solar cells. *Nature* **2015,** *517* (7535), 476-480.

23. Wu, Y.; Islam, A.; Yang, X.; Qin, C.; Liu, J.; Zhang, K.; Peng, W.; Han, L., Retarding the crystallization of PbI2 for highly reproducible planar-structured perovskite solar cells via sequential deposition. *Energy Environ Sci* **2014,** *7* (9), 2934-2938.

24. Bi, D.; El-Zohry, A. M.; Hagfeldt, A.; Boschloo, G., Unraveling the Effect of PbI2 Concentration on Charge Recombination Kinetics in Perovskite Solar Cells. *ACS Photonics* **2015,** *2* (5), 589-594.

25. Zhang, T.; Guo, N.; Li, G.; Qian, X.; Zhao, Y., A Controllable Fabrication of Grain Boundary PbI2 Nanoplates Passivated Lead Halide Perovskites for High Performance Solar Cells. *Nano Energy 26*, 50-56.

26. Chang, J.; Zhu, H.; Xiao, J.; Isikgor, F. H.; Lin, Z.; Hao, Y.; Zeng, K.; Xu, Q.-H.; Ouyang, J., Enhancing the planar heterojunction perovskite solar cell performance through tuning the precursor ratio. *J. Mater. Chem. A* **2016,** *4* (20), 7943-7949.

27. Zheng, Z.; Liu, A.; Wang, S.; Wang, Y.; Li, Z.; Lau, W. M.; Zhang, L., In situ growth of epitaxial lead iodide films composed of hexagonal single crystals. *J. Mater. Chem.* **2005,** *15* (42), 4555-4559.

28. Liu, X.; Ha, S. T.; Zhang, Q.; de la Mata, M.; Magen, C.; Arbiol, J.; Sum, T. C.; Xiong, Q., Whispering Gallery Mode Lasing from Hexagonal Shaped Layered Lead Iodide Crystals. *ACS Nano* **2015,** *9* (1), 687-695.

29. Yun, J. S.; Ho-Baillie, A.; Huang, S.; Woo, S. H.; Heo, Y.; Seidel, J.; Huang, F.; Cheng, Y.-B.; Green, M. A., Benefit of Grain Boundaries in Organic–Inorganic Halide Planar Perovskite Solar Cells. *The J. Phys. Chem. Lett.* **2015,** *6* (5), 875-880.

30. Manser, J. S.; Kamat, P. V., Band filling with free charge carriers in organometal halide perovskites. *Nat. Photon.* **2014,** *8* (9), 737-743.

31. Chen, S.; Wen, X.; Sheng, R.; Huang, S.; Deng, X.; Green, M. A.; Ho-Baillie, A., Mobile Ion Induced Slow Carrier Dynamics in Organic–Inorganic Perovskite CH3NH3PbBr3. *ACS Appl. Mater. Interfaces* **2016,** *8* (8), 5351-5357.
32. Wen, X.; Yu, P.; Toh, Y.-R.; Lee, Y.-C.; Huang, K.-Y.; Huang, S.; Shrestha, S.; Conibeer, G.; Tang, J., Ultrafast electron transfer in the nanocomposite of the graphene oxide-Au nanocluster with graphene oxide as a donor. *J. Mater. Chem. C* **2014,** *2* (19), 3826-3834.
33. Saba, M.; Cadelano, M.; Marongiu, D.; Chen, F.; Sarritzu, V.; Sestu, N.; Figus, C.; Aresti, M.; Piras, R.; Geddo Lehmann, A.; Cannas, C.; Musinu, A.; Quochi, F.; Mura, A.; Bongiovanni, G., Correlated electron–hole plasma in organometal perovskites. *Nat Commun.* **2014,** *5*, 5049.
34. Wen, X.; Feng, Y.; Huang, S.; Huang, F.; Cheng, Y.-B.; Green, M.; Ho-Baillie, A., Defect trapping states and charge carrier recombination in organic-inorganic halide perovskites. *J. Mater. Chem. C* **2016,** *4* (4), 793-800.
35. de Quilettes, D. W.; Vorpahl, S. M.; Stranks, S. D.; Nagaoka, H.; Eperon, G. E.; Ziffer, M. E.; Snaith, H. J.; Ginger, D. S., Impact of microstructure on local carrier lifetime in perovskite solar cells. *Science* **2015,** *348* (6235), 683-686.
36. Tang, J.; Kemp, K. W.; Hoogland, S.; Jeong, K. S.; Liu, H.; Levina, L.; Furukawa, M.; Wang, X.; Debnath, R.; Cha, D.; Chou, K. W.; Fischer, A.; Amassian, A.; Asbury, J. B.; Sargent, E. H., Colloidal-quantum-dot photovoltaics using atomic-ligand passivation. *Nat. Mater.* **2011,** *10* (10), 765-771.

TOC

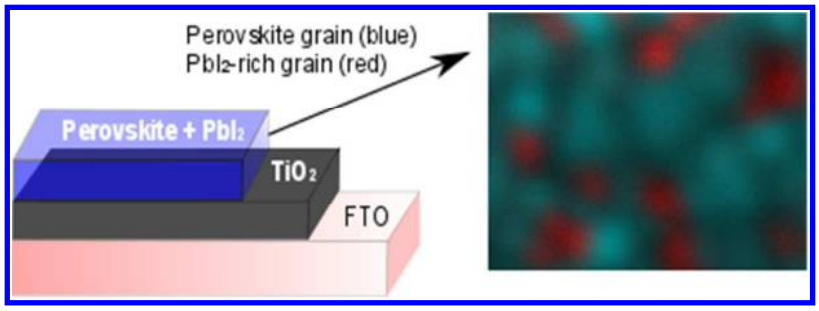
Perovskite grain (blue)
PbI2-rich grain (red)
Perovskite + PbI2
TiO2
FTO